REGULAR ARTICLE

blood advances

Redundant mechanisms driven independently by RUNX1 and GATA2 for hematopoietic development

Erica Bresciani,[1] Blake Carrington,[2] Kai Yu,[1] Erika M. Kim,[1] Tao Zhen,[1] Victoria Sanchez Guzman,[1] Elizabeth Broadbridge,[1] Kevin Bishop,[2] Martha Kirby,[3] Ursula Harper,[4] Stephen Wincovitch,[5] Stefania Dell'Orso,[6] Vittorio Sartorelli,[7] Raman Sood,[1,2] and Paul Liu[1]

[1]Oncogenesis and Development Section; [2]Zebrafish Core; [3]Flow Cytometry Core; [4]Genomics Core; [5]Cytogenetics and Microscopy Core, National Human Genome Research Institute, National Institutes of Health, Bethesda, MD; [6]Next Generation Sequencing Unit, Office of Science and Technology; [7]Laboratory of Muscle Stem Cells and Gene Regulation, National Institute of Arthritis and Musculoskeletal and Skin Diseases, National Institutes of Health, Bethesda, MD

Key Points

- RUNX1-independent mechanisms exist for the generation of HSCs and the development of functional definitive hematopoietic cells.
- GATA2 and RUNX1 functionally complement each other for their respective roles during hematopoiesis.

RUNX1 is essential for the generation of hematopoietic stem cells (HSCs). *Runx1*-null mouse embryos lack definitive hematopoiesis and die in mid-gestation. However, although zebrafish embryos with a *runx1* W84X mutation have defects in early definitive hematopoiesis, some *runx1*$^{W84X/W84X}$ embryos can develop to fertile adults with blood cells of multilineages, raising the possibility that HSCs can emerge without RUNX1. Here, using 3 new zebrafish *runx1*$^{-/-}$ lines, we uncovered the compensatory mechanism for *runx1*-independent hematopoiesis. We show that, in the absence of a functional *runx1,* a *cd41*-green fluorescent protein (GFP)$^{+}$ population of hematopoietic precursors still emerge from the hemogenic endothelium and can colonize the hematopoietic tissues of the mutant embryos. Single-cell RNA sequencing of the *cd41*-GFP^{+} cells identified a set of *runx1*$^{-/-}$-specific signature genes during hematopoiesis. Significantly, *gata2b,* which normally acts upstream of *runx1* for the generation of HSCs, was increased in the *cd41*-GFP^{+} cells in *runx1*$^{-/-}$ embryos. Interestingly, genetic inactivation of both *gata2b* and its paralog *gata2a* did not affect hematopoiesis. However, knocking out *runx1* and any 3 of the 4 alleles of *gata2a* and *gata2b* abolished definitive hematopoiesis. *Gata2* expression was also upregulated in hematopoietic cells in *Runx1*$^{-/-}$ mice, suggesting the compensatory mechanism is conserved. Our findings indicate that RUNX1 and GATA2 serve redundant roles for HSC production, acting as each other's safeguard.

Introduction

The emergence and maintenance of hematopoietic stem cells (HSCs) is regulated by several transcription factors including RUNX1 and GATA2.[1-8] *Gata2* is expressed in all functional HSCs and most hematopoietic progenitor cells.[9] Mouse *Gata2*$^{-/-}$ embryos are defective in definitive hematopoiesis and die at E10.5.[6] Moreover, *Gata2* is required for the generation of HSCs during the stage of endothelial to hematopoietic cell transition in the aorta gonad mesonephric region (AGM).[8] *GATA2* is also frequently involved in human leukemia, and germline mutations in *GATA2* are associated with an autosomal dominant disease with recurrent infections, myelodysplastic syndrome, and predisposition to leukemia.[10]

Runx1$^{-/-}$ mice lack all definitive blood lineages and die in midgestation.[2] *Runx1* is also required for HSC formation during embryo development.[11] Recent studies have shown that HSC precursors form but do not

Submitted 4 December 2020; accepted 2 June 2021; prepublished online as *Blood Advances* First Edition 7 September 2021; final version published online 30 November 2021. DOI 10.1182/bloodadvances.2020003969.

For original data, please contact pliu@nih.gov. RNA-seq data has been deposited in Gene Expression Omnibus (GEO) (#GSE158101). Raw data has also been deposited into the GEO (GSE158098 and GSE169689).

The full-text version of this article contains a data supplement.

further develop into HSCs in *Runx1*-deficient mice.[12] Our group previously generated a zebrafish line with a truncation mutation in *runx1* (*runx1*$^{W84X/W84X}$).[13,14] Similar to *Runx1*$^{-/-}$ mice, *runx1*$^{W84X/W84X}$ embryos failed to develop definitive hematopoiesis. Surprisingly, 20% of the *runx1*$^{W84X/W84X}$ larvae could recover definitive hematopoiesis and survive to adult.[14] These findings suggested that HSCs could form without RUNX1 in the zebrafish. However, given the nature of the W84X mutation and the fact that *runx1*^{W84X} messenger RNA (mRNA) was still expressed in the *runx1*$^{W84X/W84X}$ fish, we could not exclude the possibility of functional RUNX1 protein production through a stop-codon readthrough mechanism during translation.

We believe that elucidating the mechanism of this RUNX1-independent hematopoiesis has far-reaching implications in developing therapeutics for acute myeloid leukemia with germline or somatic mutations in RUNX1. Therefore, we generated 3 new *runx1*$^{-/-}$ lines to uncover the mechanism of this RUNX1-independent production of HSCs. We detected *cd41*:green fluorescent protein (GFP)$^{+}$ HSCs/hematopoietic stem and progenitor cells (HSPCs) in the *runx1*$^{-/-}$ embryos and characterized their expression profile by single-cell RNA sequencing (scRNA-seq). Interestingly, our analysis identified *gata2b* as 1 of the signature genes of *runx1*-independent HSC/HSPCs. We generated new *gata2b* and *gata2a* mutant lines and crossed them to the *runx1*$^{-/-}$ lines to probe the interplay between RUNX1 and GATA2. Our findings suggest that RUNX1 and GATA2 act redundantly to support the formation and maintenance of HSCs and a functional hematopoietic system.

Methods

Zebrafish lines and maintenance

All zebrafish experiments were performed in compliance with National Institutes of Health guidelines for animal handling and research. Zebrafish handling and breeding were performed as described previously.[15] The following zebrafish strains were used: wild-type zebrafish strain EK (Ekkwill) and TAB5, Tg(*gata1*:dsRed),[16] *Tg(cd41*:GFP),[17] and *Tg(kdrl:mCherry)*.[18] All animals and procedures used in this study were approved by the National Human Genome Research Institute Animal Care and Use Committee.

runx1, *gata2a*, and *gata2b* mutant generation and genotyping

Zebrafish mutants were generated with transcription activator-like effector nucleases (TALENS; *runx1* ^{del8} and *runx1* ^{del25}) or clustered regularly interspaced short palindromic repeats (CRISPR)/Cas9 (*runx1* del[e3-8], *gata2a*, and *gata2b* mutants). The TALEN and sgRNA sequences, target exons, and genotyping primer sequences for all mutations are described in supplemental Table 1 and in the supplemental Methods.

Kidney RNA extraction and RNA sequencing

Kidneys were dissected from approximately 2.5-month-old fish. See supplemental Methods for detailed dissociation protocol. RNA sequencing was performed on the HiSeq 2500 (Illumina) using paired-end library preparation (TruSeq RNA Library Prep Kit v2) at the National Institutes of Health Intramural Sequencing Center. Low-quality sequencing reads were removed with in-house script. RNA-Seq reads were aligned to the zebrafish genome reference (GRCz11) and transcript reference (GRCz11.99) using hisat2 (v2.2.1.0)[19] on National Institutes of Health high performance computing (HPC) Biowulf cluster (http://hpc.nih.gov). We used htseq-count (v0.11.4)[20] to generate gene expression estimates. DESeq2[21] (version 3.4.2, http://www.r-project.org/) was used for differential gene expression analysis. Gene ontology enrichment analysis was performed using Metascape (http://metascape.org).[21] Raw data have been deposited to GEO (GSE158098 and GSE169689).

Fluorescence-activated cell sorting and single-cell capture and sequencing with 10× Genomics chromium

Wild-type and *runx1*$^{del8/del8}$ embryos were collected at 2.5, 6, 10, and 16 day postfertilization (dpf), and GFP^{+} cells were sorted on a fluorescence-activated cell sorter (FACS) AriaIII (Becton Dickinson, Franklin Lakes, NJ). GFP^{low} cells were loaded on a chromium instrument (10× Genomics, Pleasanton, CA) to generate single-cell gel beads in emulsion (GEMs). Single-cell RNA-seq libraries were prepared using chromium single-cell 3′ Library & Gel Bead Kit v3 (P/N1000075; 10× Genomics). The barcode sequencing libraries were sequenced on Illumina HiSeq2500/HiSeq3000.

Data processing, clustering, and trajectory analysis

Sequences from the chromium platform were demultiplexed and aligned using CellRanger v2.0.2 from 10× Genomics using zebrafish reference genome (GRCz10) and transcript annotation reference (GRCz10.87). Clustering, filtering, variable gene selection, and dimensionality reduction were performed using the Seurat v3.1.4.[22,23] Raw data matrices of 2 or more Seurat objects were merged to generate a new Seurat object with the resulting combined raw data matrix. The cell identities of the clusters were reassigned based on the expression of well-established hematopoietic markers that were identified by our unbiased analysis as cluster signature genes. The expression of signature markers that identify different cell identities is presented, for each time point, in heatmaps and feature maps (see Figures 3 and 4; supplemental Figures 2-4).

We applied single-cell trajectories reconstruction, exploration and mapping (STREAM, version 1.0)[24] software with single-cell gene expression matrix exported from Seurat to reconstruct the trajectories of different cell types. Different correlation metrics were used to calculate the ranks of cells, which reflect the cell position over the pseudotime axis. scRNA-seq data have been deposited in GEO (GSE158099). More details about data processing, clustering, and trajectory analysis can be found in the supplemental Methods.

Mouse cell preparation and RNA sequencing

All mice and procedures used in this study were approved by the National Human Genome Research Institute Animal Care and Use Committee. *Runx1* conditional knockout (*Runx1*$^{f/f}$),[25] *Mx1-Cre*,[26] and β-actin-Cre recombinase transgenic (Actb-Cre^{+})[27] mice have been described previously. RNA sequencing was performed on mRNA isolated from c-Kit^{+} bone marrow cells of mice.[28] Quantitative polymerase chain reaction was performed on mRNA extracted from whole aorta-gonad-mesonephros (AGM) of E10.5 embryos. Details on the procedures and data analysis are provided in the supplemental Methods. Sequencing data have been deposited at GEO (GSE158100).

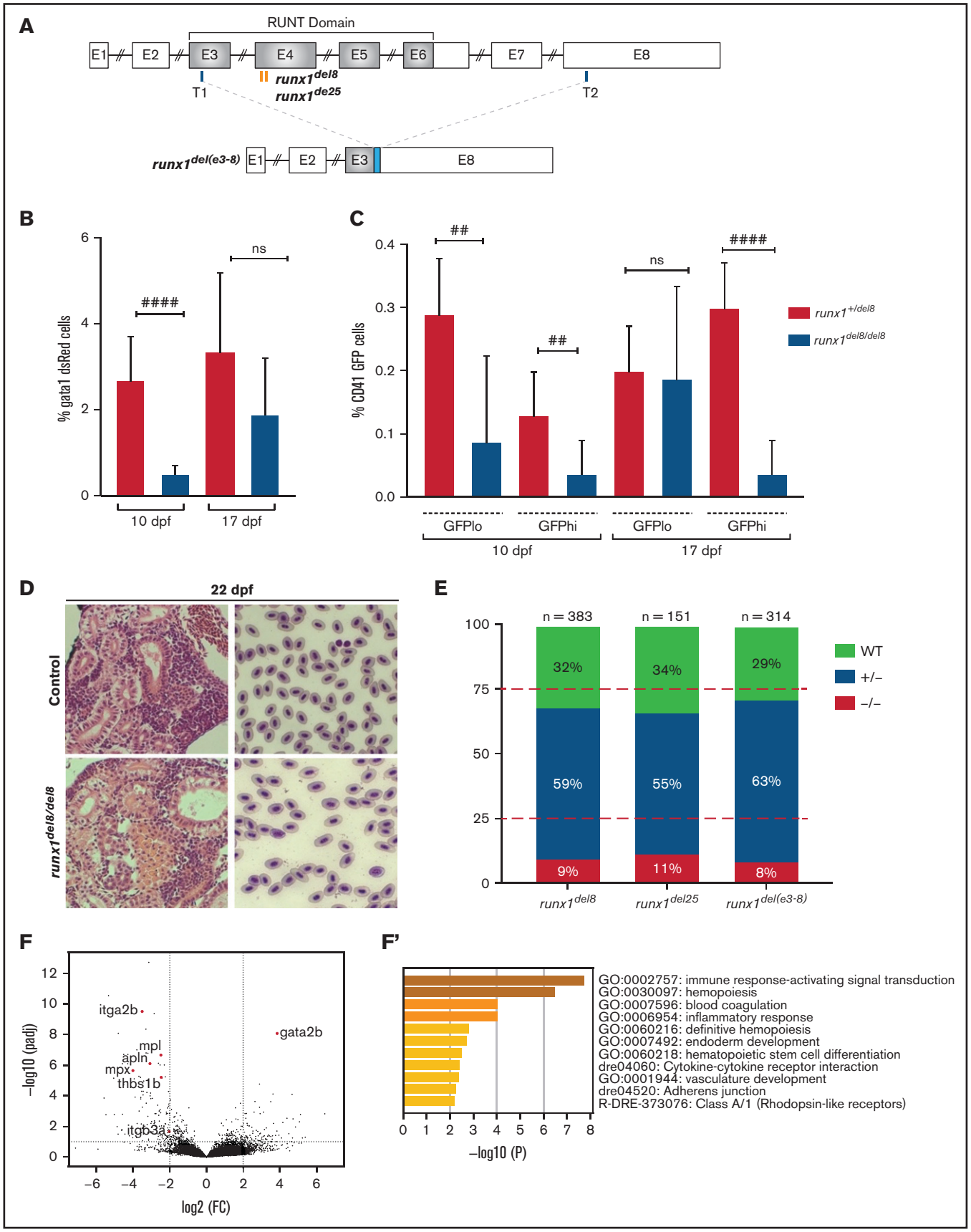
A
RUNT Domain
E1
E2
E3
E4
E5
E6
E7
E8
T1
T2
runx1del8
runx1de25
runx1del(e3-8)
B
% gata1 dsRed cells
####
ns
10 dpf
17 dpf
C
% CD41 GFP cells
##
##
ns
####
GFPlo
GFPhi
GFPlo
GFPhi
10 dpf
17 dpf
runx1+/del8
runx1del8/del8
D
22 dpf
Control
runx1del8/del8
E
n = 383
n = 151
n = 314
32%
34%
29%
59%
55%
63%
9%
11%
8%
WT
+/–
–/–
runx1del8
runx1del25
runx1del(e3-8)
F
–log10 (padj)
log2 (FC)
itga2b
gata2b
mpl
apln
mpx
thbs1b
itgb3a
F'
–log10 (P)
GO:0002757: immune response-activating signal transduction
GO:0030097: hemopoiesis
GO:0007596: blood coagulation
GO:0006954: inflammatory response
GO:0060216: definitive hemopoiesis
GO:0007492: endoderm development
GO:0060218: hematopoietic stem cell differentiation
dre04060: Cytokine-cytokine receptor interaction
GO:0001944: vasculature development
dre04520: Adherens junction
R-DRE-373076: Class A/1 (Rhodopsin-like receptors)

Figure 1.

Results

Demonstration of RUNX1-independent hematopoiesis in 3 new *runx1* mutant lines

To investigate whether RUNX1-independent emergence of HSCs exists, we generated 3 new *runx1*$^{-/-}$ lines (Figure 1A; supplemental Figure 1A-D). Using TALENs, we obtained zebrafish lines with an 8-bp deletion and a 25-bp deletion (*runx1*^{del8} and *runx1*^{del25}) within exon 4 of *runx1* (Figure 1A; supplemental Figure 1A; supplemental Table 1). These mutations are predicted to cause frameshifts and premature terminations within the runt-homology domain (RHD), resulting in loss of function (supplemental Figure 1B; supplemental Table 2). Because *runx1* mRNA was still detectable in *runx1*$^{del8/del8}$ and *runx1*$^{del25/del25}$ embryos (supplemental Figure 1C), we used 2 CRISPR-guide RNAs (supplemental Table 1), targeting exon 3 (encoding RHD) and exon 8 (the last coding exon of *runx1*), respectively, to establish a mutant line carrying an exon 3 to 8 deletion (*runx1*$^{del(e3-8)/del(e3-8)}$; Figure 1A; supplemental Figure 1A-B,D; supplemental Table 2), in which *runx1* full-length transcript was not detectable (supplemental Figure 1C-D).

Whole-mount in situ hybridization showed lack of expression of all definitive hematopoietic markers (*c-myb, mpx, hbae1, rag1*) between 3 and 5 dpf in these 3 *runx1* mutant lines (supplemental Figure 1E), indicating complete failure of definitive hematopoiesis at this stage. The larvae from all 3 *runx1* mutant lines were followed and found to undergo a bloodless phase between 10 and 16 dpf; during this time, some of the *runx1* mutant larvae died. Circulating blood cells started to reappear in the remaining *runx1* mutant larvae between 16 and 20 dpf, and by 22 dpf, all the surviving *runx1* mutant larvae had blood circulation. The hematopoietic defects in these 3 mutant lines were qualitatively and quantitatively similar with each other. For practical reasons, we focused our subsequent studies on the *runx1*^{del8} mutant line.

Flow cytometric analysis showed significant reductions of *dsRed*$^{+}$ erythrocytes and GFP^{high} thrombocytes in the Tg(*gata1:dsRed; cd41:GFP*) *runx1*$^{del8/del8}$ larvae at 10 dpf (Figure 1B-C). Interestingly, the GFP^{low} HSC/HSPC population was decreased in the mutants but still detectable (Figure 1C). At 17 dpf, when circulating blood cells started to reappear in the *runx1*$^{del8/del8}$ larvae, *dsRed*$^{+}$ erythrocytes and GFP^{low} HSC/HSPCs increased correspondingly but not the GFP^{high} thrombocytes (Figure 1B-C). At 22 dpf, the kidneys in the *runx1*$^{del8/del8}$ larvae were filled with blood progenitors, comparable to the controls and blood smear showed normal erythroid cells (Figure 1D). Eventually, 8% to 11% of the adult fish from *runx1*$^{+/-}$ incrosses were *runx1*$^{-/-}$ (Figure 1E). *runx1*$^{-/-}$ adults had normal size and morphology (supplemental Figure 1F). Overall, our data strongly suggest that in the absence of RUNX1, there is an independent mechanism for HSC formation.

Gene expression changes in adult *runx1*-null hematopoietic cells

To assess gene expression profile of hematopoietic cells in *runx1*$^{-/-}$ adults, we performed RNA-seq on dissected kidneys from both *runx1*^{del8} and *runx1*^{del25} (~2.5 months old, n = 3 *runx1*^{del25}, n = 3 wild-type siblings; n = 2 *runx1*^{del8} and n = 3 wild-type siblings). Only 140 differentially expressed (DE) genes (107 downregulated and 33 upregulated; $P_{adj} < .05$, fold change [FC] > 2) were detected between mutant and wild type (Figure 1F; supplemental Table 3). Gene ontology enrichment analysis showed over-representation of genes related to immune response signaling/inflammation and blood coagulation and hematopoiesis (Figure 1F′). Indeed, key thrombocyte genes such as *itga2b* (*cd41*), *mpl, thbs1b*, *apln*, and *itgb3a* (*cd61*)[29] were downregulated, indicating defects in thrombopoiesis in *runx1*$^{-/-}$ fish (Figure 1F). The myeloid markers *mpx* and *lyz* were also downregulated, suggesting an impairment of neutrophils. Interestingly, the HSC transcription factor *gata2b* was upregulated in *runx1*$^{-/-}$ fish (Figure 1F). Our results suggest that adult hematopoiesis in *runx1*$^{-/-}$ fish is largely intact and multilineage.

cd41-GFP^{+} HSC/HSPCs are formed in *runx1*$^{-/-}$ embryos

Our analysis of Tg(*gata1:dsRed; cd41:GFP*) *runx1*$^{del8/del8}$ embryos showed the presence of cd41:GFP^{low} HSC/HSPCs at 10 dpf, which were expanded during hematopoietic recovery. To identify where and when *runx1*-independent hematopoietic precursors might arise, we generated *runx1*$^{del8/del8}$*;Tg(cd41:GFP);Tg(kdrl:mCherry)* embryos. Interestingly, at ~52 hour postfertilization (hpf), we could detect *cd41*-GFP^{+} mCherry^{+} cells in the AGM of *runx1*$^{del8/del8}$ embryos, indicating that these cells were derived from hemogenic endothelium (Figure 2A). Moreover, time-lapse confocal analysis showed that the *cd41*-GFP^{+} cells in the *runx1*$^{del8/del8}$ embryos retained HSC behavior as they were released from the AGM into the circulation, similar to *cd41*-GFP^{+} HSCs in the wild-type embryos (supplemental Movies 1 and 2). At 3 dpf, *cd41*-GFP^{+} cells had colonized the caudal hematopoietic tissue (CHT) of the *runx1*$^{del8/del8}$ embryos (Figure 2B); however, residual GFP^{+} cells could be found in the AGM (Figure 2C), suggesting that the emergence/release of the HSPC in *runx1*$^{-/-}$ was slower than normal. In addition, flow cytometric analysis showed that the number of *cd41*-GFP^{low} cells at 2.5 dpf in the *runx1*$^{del8/del8}$ was lower than normal (supplemental Figure 2A-B).

The transcriptional profile of wild-type and *runx1*$^{-/-}$ HSC/HSPCs was analyzed by scRNA-seq on *cd41*-GFP^{low} cells at 2.5 dpf (supplemental Figure 2C). Uniform manifold approximation and projection (UMAP) of merged wild-type and *runx1*$^{del8/del8}$ *cd41*-GFP^{low} cells defined 11 clusters (Figure 3A; supplemental Table 4). Cell identities were assigned to each cluster based on well-established lineage markers identified as clusters signatures (supplemental Table 4).

Figure 1. *runx1*$^{-un}$ mutants survive to adult and recover multilineage hematopoiesis. (A) Schematic representation of the *runx1* gene showing the regions (orange bars) targeted with engineered TALENs that generated the *runx1*^{del8}, runx1^{del25} mutant lines and the CRISPR targets, T1 and T2 (blue bars), used to generate the *runx1*$^{del(e3-8)}$ mutant line as shown in the lower panel. The cyan box in the lower panel indicates a 66-bp insertion between the 2 cut sites. Percentage of *gata1:dsRed*$^{+}$ (B) and *cd41*:GFP^{low} or *cd41*:GFP^{high} (C) in Tg(*gata1:dsRed; cd41:GFP*) *runx1*$^{del8/del8}$ *runx1*$^{+/del8}$ controls at 10 and 17 dpf analyzed by flow cytometry ($^{\#\#}P < .01$, $^{\#\#\#\#}P < .0001$). (D) Kidney histology and blood smear of a representative 22 dpf *runx1*$^{del8/del8}$ appear similar to a *runx1*$^{+/del8}$ control sibling. (E) Stacked bar chart showing the percentage of adult *runx1*$^{del/del8}$, *runx1*$^{del2/del25}$, and *runx1*$^{del(e3-8)/del(e3-8)}$ recovered from inbred heterozygous parents; red dashed lines indicate the expected Mendelian ratio. (F) Volcano plot showing the differentially expressed genes in the kidneys between adult *runx1*$^{-un}$ and wild-type zebrafish. The red dots identify known hematopoietic markers for thrombocytes, myeloid cells, and HSCs that are differentially expressed at FC > 2 and $P_{adj} < .05$. (F′) Gene ontology enrichment analysis results for panel F.

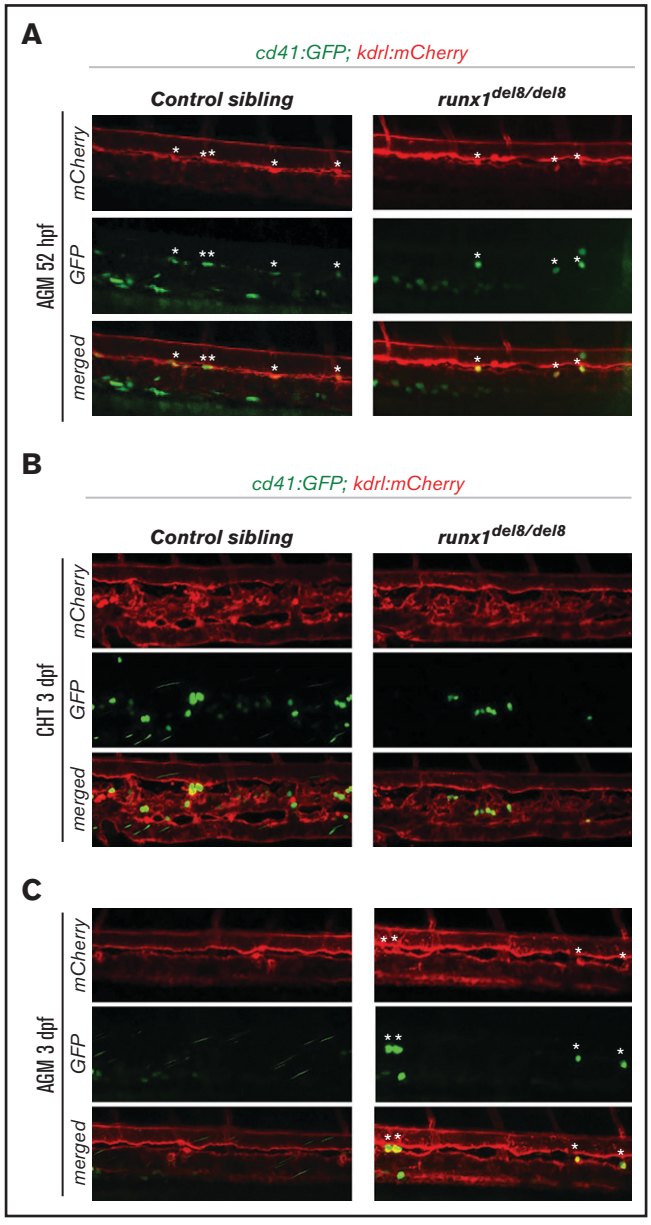

Figure 2. Development of *cd41*:GFP^{+} hematopoietic precursors in *runx1*$^{del8/del8}$ AGM and CHT. (A) Snapshots of the AGM region of *runx1*$^{del8/del8}$ and control sibling *Tg(cd41:GFP); Tg(kdrl:mCherry)* at 52 hours postfertilization (hpf), obtained from time-lapse recordings on a confocal microscope (supplemental Movies 1 and 2). *cd41*:GFP^{+} mCherry^{+} double-positive cells are indicated with white asterisks. (B-C) Live confocal imaging of the CHT (B) and AGM (C) regions in the *Tg(cd41:GFP);* (B) *Tg(kdrl:mCherry)* embryos at 3 dpf. *cd41*:GFP^{+} cells are found in the CHT. (C) Residual *cd41*:GFP^{+} cells (white asterisks) are still detectable in the AGM of *runx1*$^{del8/del8}$.

Although the nonhematopoietic clusters were composed of mixed genotypes, the hematopoietic clusters were mainly composed of wild-type cells, indicating a reduction in the hematopoietic *cd41*-GFP^{low} cells in *runx1*$^{-/-}$ (Figure 3A-B). The hematopoietic subpopulations expressed known markers for HSCs/HSPCs, multipotent progenitors, and erythroid and myeloid progenitors, which likely represent *erythro*-myeloid progenitors generated at earlier stages of development and are known to be *cd41*:GFP^{+}[30] (Figure 3C-D; supplemental Figure 2D).

Interestingly, both clusters 2 and 8 expressed HSC/HSPC signature genes such as *fli1a*, *tal1* (also known as *scl)*, *c-myb,* and *lmo2* (Figure 3A,C-D; supplemental Figure 2D). These 2 populations segregated based on their genotype with cluster 2 mainly composed of wild type and cluster 8 mainly *runx1*$^{del8/del8}$ (Figure 3A-B). Only 41 DE genes were identified between clusters 2 and 8 (FC $>$ 2, $P_{adj} <$ .001; supplemental Table 4), suggesting that the *runx1*$^{del8/del8}$ HSC/HSPC population was not too different from wild type.

runx1$^{-/-}$ HSCs/HSPCs at larval stages had a distinct gene expression profile

To uncover the compensatory mechanism that drive the hematopoietic recovery in *runx1*$^{-/-}$, we characterized the expression profile of *cd41*-GFP^{low} cells during larval development by scRNA-seq (supplemental Figure 3A-B). UMAPs of merged wild type and *runx1*$^{-/-}$ at 6 dpf identified multiple hematopoietic subpopulations, highlighting the level of heterogeneity of *cd41*-GFP^{low} cells at this stage (Figure 4A; supplemental Table 5). HSCs/HPSCs (clusters 1, 3, and 5) expressing markers such as *tal1*, *lmo2*, and *c-myb* (Figure 4C; supplemental Figure 3C) again segregated based on genotype (cluster 1 wild type; cluster 3 mutant; Figure 4A-C). Cluster 5, again predominantly wild type, was composed of HSCs undergoing cell division as shown by the specific expression of cell cycle markers *ccna2* and *ccnb1* (Figure 4C). Notably, *meis1b, fli1a*, and *gata2b* were among the signature markers for the *runx1*$^{del8/del8}$ HSC/HSPCs (Figure 4C; supplemental Figure 3C).

At 10 dpf, wild-type and mutant *cd41*-GFP^{low} cells again clustered separately (Figure 4E). For the first time, the *runx1*$^{del8/del8}$ cells showed a higher degree of heterogeneity with *runx1*$^{del8/del8}$ specific HSC/HSPCs and erythroid progenitors clusters, and 1 myeloid progenitor population shared with wild type (Figure 4D-F; supplemental Figure 3D). At this stage, *meis1b, fli1a*, and *gata2b* remained specifically expressed in the *runx1*$^{del8/del8}$ HSC/HSPCs (Figure 4F; supplemental Figure 3D; supplemental Table 5).

At 16 dpf, the *runx1*$^{-/-}$ larvae were separated based on their phenotype: bloodless (without circulating blood cells) and recovered (regained some or nearly normal levels of circulating blood cells). This large dataset of ~11 000 *runx1*$^{del8/del8}$ cells presented 5 hematopoietic populations and showed complete overlap between bloodless and recovered (supplemental Figure 4A-C; supplemental Table 5), suggesting these larvae had the same hematopoietic progression despite the phenotypic difference.

Analysis of a merged dataset containing wild-type and *runx1*$^{del8/del8}$ (bloodless and recovered) *cd41*-GFP^{low} cells at 16 dpf showed again that most cells clustered based on their genotypes (Figure 4G-I; supplemental Table 5). Importantly, the wild-type and *runx1*$^{del8/del8}$ HSC/HSPC clusters were distinct from each other. There were 2 *runx1*$^{del8/del8}$-specific erythroid clusters (clusters 0 and 8) expressing different levels of *gata1a, urod*, *hbae1*, *hbaa1*, and *alas2* (Figure 4G-I; supplemental Figure 4D). On the other hand, multipotent progenitor cluster (cluster 1) was mostly composed of wild-type cells. Only the myeloid clusters 4 and 10 were shared by wild-type and *runx1*$^{del8/del8}$ cells (Figure 4G-I; supplemental Figure 4D). Overall, our data suggest that the HSC population in the *runx1*$^{del8/del8}$ larvae, although different

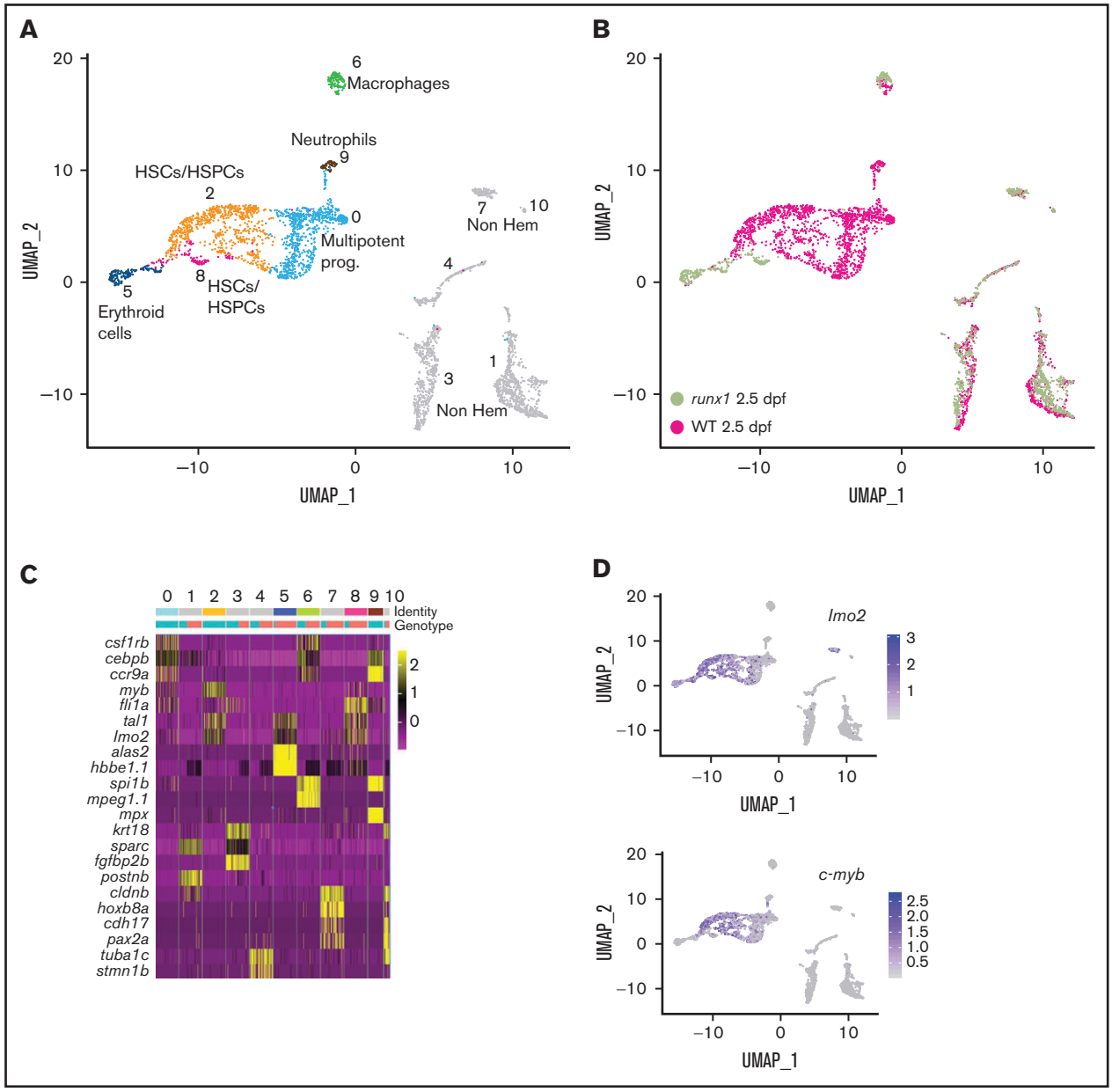

Figure 3. Single-cell gene expression profile of wild-type and *runx1*$^{del8/de}$ *cd41*:GFP^{low} hematopoietic precursors at 2.5 dpf. (A) UMAP of freshly FACS-isolated *cd41*:GFP^{low} cells from wild-type and *runx1*$^{del8/del8}$ embryos at 2.5 dpf. Colored clusters represent hematopoietic cells; gray clusters are nonhematopoietic (based on expression profile). (B) UMAP depicting the genotypes of the *cd41*:GFP^{low} cells. Mint dots, wild type; magenta dots, *runx1*$^{del8/del8}$. (C) Heat map depicting the expression of signature genes representative of different cell identities. The horizontal bars on the top correspond to the clusters identified in panel A (Identity) and show the distribution of the 2 genotypes (Genotype) across the clusters. One hundred representative cells per clusters are shown. (D) Feature plots depicting the expression level of the HSC markers *c-myb* and *lmo2* (purple is high, gray is low). See also supplemental Figure 2 for additional scRNA-seq data from 2.5-dpf embryos.

from the wild type, could give rise to erythroid and myeloid progenitors, but a multiprogenitor population was not established at this stage.

Comparing the hematopoietic differentiation trajectories in *runx1*$^{del8/del8}$ and wild-type larvae

With the aim to reconstruct the progression of the hematopoietic recovery in the *runx1*$^{del8/del8}$ larvae, we merged scRNA-seq datasets from 6, 10, and 16 dpf based on genotype (supplemental Figure 5A-B,D-E; supplemental Table 6) and performed trajectory analysis (STREAM[24]).

The unbiased trajectory reconstruction of wild-type *cd41* GFP^{low} cells (11 683 cells) identified 8 different branches (Figure 5A; supplemental Figure 5C). The HSC/HSPCs were split in 3 arms (arms S2-S0, S2-S4, S2-S5; Figure 5A-B; supplemental Figure 5C). Arm S2-S0

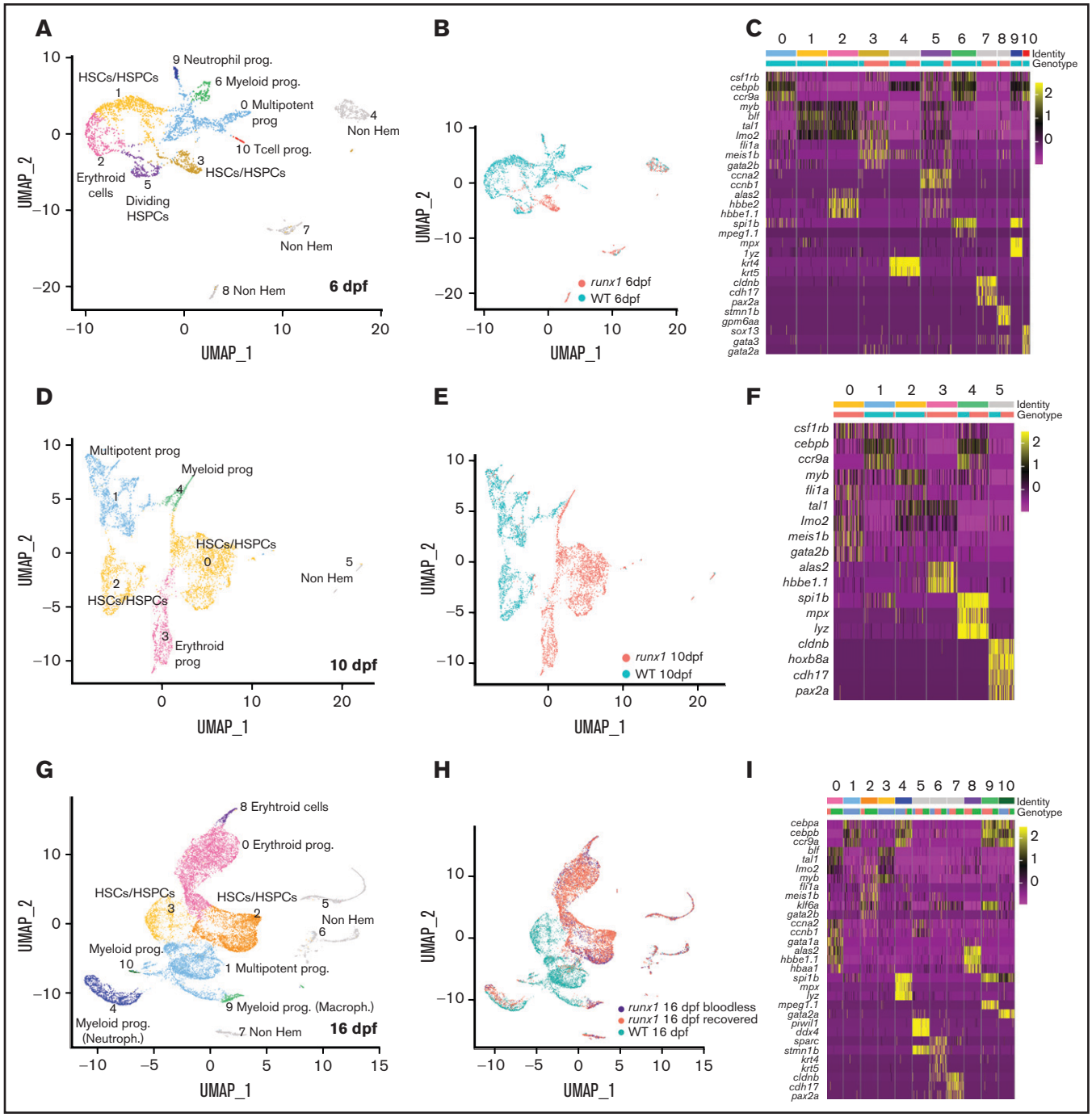

Figure 4. Single-cell analysis of wild-type and *runx1*$^{del8/del8}$ *cd41*:GFP^{low} at 6, 10, and 16 dpf show only few overlapping populations. UMAP of freshly FACS-isolated *cd41*:GFP^{low} cells from wild-type and *runx1*$^{del8/del8}$ embryos at 6 (A), 10 (D), and 16 dpf (G). Colored clusters represent hematopoietic cells; gray clusters are nonhematopoietic (based on expression profile). UMAP depicting the genotypes of the *cd41*:GFP^{low} cells at 6 (B), 10 (E), and 16 (H). Mint dots, wild type; magenta dots, *runx1*$^{del8/del8}$ (B,E). At 16 dpf, mint dots represent wild type; magenta dots, *runx1*$^{del8/del8}$ with circulating blood cells (recovered); blue dots, bloodless *runx1*$^{del8/del8}$. (C,F,I) Heat maps depicting the expression of signature genes representative of different cell identities in each of the clusters identified, respectively, in panels A, D, and G. The horizontal bars on the top correspond to the clusters identified the correspondent UMAP (Identity) and show the distribution of the 2 genotypes (Genotype) across the clusters. One hundred representative cells per clusters are shown. See also supplemental Figures 3 and 4 for additional scRNA-seq data.

was composed largely by HSCs/HSPCs at 10 and 16 dpf; S2-S4 was populated by HSCs/HSPCs from 10 dpf differentiating into erythroid progenitors expressing *gata1, alas2*, and embryonic globins (eg, *hbbe1*; Figure 5A-B; supplemental Figure 5C,G). Arm S2-S5 cells were exclusive of 16 dpf (Figure 5A-B) and expressed adult globin *hbaa1,* suggesting these cells were responsible for the switch from embryonic to adult erythropoiesis[31] (Figure 5A-B; supplemental Figure 5C,G). Cells in the S0-S1 branch were derived from *cd41-*

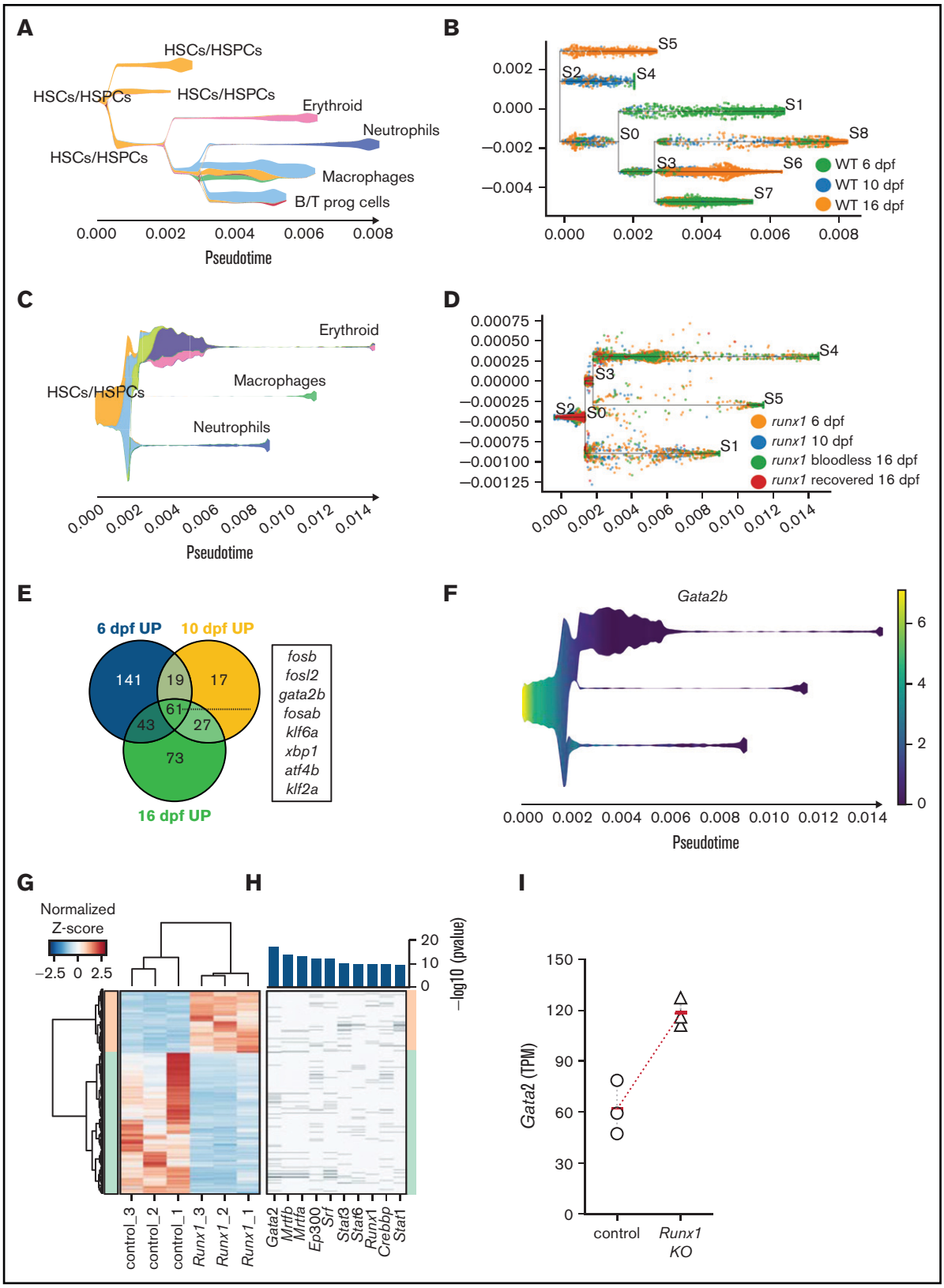
A
HSCs/HSPCs
HSCs/HSPCs
HSCs/HSPCs
HSCs/HSPCs
Erythroid
Neutrophils
Macrophages
B/T prog cells
0.000 0.002 0.004 0.006 0.008
Pseudotime
B
S5
S2
S4
S1
S0
S8
S3
S6
S7
WT 6 dpf
WT 10 dpf
WT 16 dpf
0.002
0.000
−0.002
−0.004
0.000 0.002 0.004 0.006 0.008
C
Erythroid
Macrophages
HSCs/HSPCs
Neutrophils
0.000 0.002 0.004 0.006 0.008 0.010 0.012 0.014
Pseudotime
D
0.00075
0.00050
0.00025
0.00000
−0.00025
−0.00050
−0.00075
−0.00100
−0.00125
S4
S3
S5
S2
S0
S1
runx1 6 dpf
runx1 10 dpf
runx1 bloodless 16 dpf
runx1 recovered 16 dpf
0.000 0.002 0.004 0.006 0.008 0.010 0.012 0.014
E
6 dpf UP
10 dpf UP
16 dpf UP
141
19
17
61
43
27
73
fosb
fosl2
gata2b
fosab
klf6a
xbp1
atf4b
klf2a
F
Gata2b
6
4
2
0
0.000 0.002 0.004 0.006 0.008 0.010 0.012 0.014
Pseudotime
G
Normalized
Z-score
−2.5 0 2.5
control_3
control_2
control_1
Runx1_3
Runx1_2
Runx1_1
H
20
10
0
−log10 (pvalue)
Gata2
Mrtfb
Mrtfa
Ep300
Srf
Stat3
Stat6
Runx1
Crebbp
Stat1
I
150
120
90
60
30
0
Gata2 (TPM)
control
Runx1
KO

Figure 5.

GFP^{low} at 6 dpf and expressed embryonic erythroid markers (Figure 5A-B; supplemental Figure 5C,G). The remaining branch of HSPCs (S0-S3) differentiates toward myeloid progenitors with macrophage signatures (S3-S7), neutrophils (S3-S8), and B/T progenitor cells (S3-S6; Figure 5A-B; supplemental Figure 5C,G).

The trajectory of *runx1*$^{del8/}$cells (16 660 cells) showed a lower number of bifurcations compared with the wild type (Figure 5C-D; supplemental Figure 5F). The *runx1*$^{del8/del8}$ cells predominantly populated the most undifferentiated branches: HSCs/HSPCs (S2-S0), HSPCs/multipotent progenitors (S2-S0, S0-S3, S0-S1), and HSPCs, which were undergoing active translation based on gene ontology term analysis (translating HSPCs, S0-S3; Figure 5C-D; supplemental Figure 5F,H; supplemental Table 6). HSPCs/multipotent progenitors and translating HSPCs also populated the erythroid trajectory branch (S3-S4), which includes erythroid progenitors with both embryonic and adult globin signatures (*hbbe1, hbbe2*, and *hbaa1*), and the myeloid branches with neutrophils (S0-S1) and macrophages signatures (S0-S5; Figure 5C-D; supplemental Figure 5F,H). Overall, the lower level of complexity and the preponderant distribution of the *runx1 cd41*-GFP^{low} cells in the more undifferentiated branches were consistent with delayed hematopoiesis in the *runx1*$^{del8/del8}$ larvae.

G*ata2* is upregulated in the HSPCs in the *Runx1* knockout zebrafish and mice

To gain insight into the compensatory mechanism taking place in *runx1*$^{-/-}$ HSCs/HSPCs, we considered the upregulated genes in the *runx1*$^{del8/del8}$ HSC/HSPCs at 6, 10, and 16 dpf (Figure 5E; supplemental Table 5). We reasoned that another transcription factor was likely responsible for compensation of *runx1*. Among 61 genes consistently upregulated in *runx1*$^{del8/del8}$ HSC/HSPCs ($P_{adj} < .05$, FC $>$ 1.5), only 8 were transcription factors (Figure 5E). Significantly, in the absence of a functional runx1, *gata2b* was the only transcription factor that remained persistently upregulated in the HSC population at larval stages and also in the adult kidney (Figures 5E-F and 1F-F′).

We also examined the expression levels of *Gata2* in the *Runx1* knockout mice to determine whether the interplay between *runx1* and *gata2* is evolutionarily conserved. *Gata2* expression level in the AGM of *Runx1* conditional knockout mouse embryos (*Runx1*$^{f/f}$, *β-actin-Cre)* at E10.5 was unchanged (supplemental Figure 6A-C). We then examined the gene expression profiles in c-Kit^{+} bone marrow HSPCs from adult *Runx1* conditional knockout mice (*Runx1*$^{-/-}$, *Mx1-Cre*; supplemental Figure 6D).[25,32] We identified a total of 1354 differentially expressed genes ($P_{adj} < .05$, FC > 2) between *Runx1*$^{-/-}$ and control c-Kit^{+} HSPCs (Figure 5G; supplemental Figure 6E; supplemental Table 7), and ingenuity pathway identified GATA2 as the top upstream regulator responsible for the gene expression changes (Figure 5H; supplemental Figure 6F). Moreover, *Gata2* expression was increased in the *Runx1*$^{-/-}$ c-Kit^{+} HSPCs with a highly significant P_{adj} (9.41E−06; Figure 5I). These findings suggest that the interplay between *Runx1* and *Gata2* is evolutionarily conserved.

gata2 is required for *runx1*-independent hematopoiesis

To determine whether *gata2b* could compensate in the absence of *runx1*, we generated 2 *gata2b* mutant lines (supplemental Table 1): a 5-bp insertion and a 7-bp deletion located upstream and within the first zinc-finger domain of GATA2, respectively (Figure 6A; supplemental Figure 7A-B; supplemental Table 2). Surprisingly both *gata2b* mutants reached adulthood according to Mendelian ratio with no hematopoietic phenotype (supplemental Figure 7C). However, when *runx1*$^{del8/del8}$ and *gata2b*$^{ins5/ins5}$ fish were bred together, *runx1*$^{del8/del8}$;*gata2b*$^{ins5/ins5}$ adults were recovered at lower than expected numbers, suggesting that *gata2b* is important for the survival of *runx1*$^{-/-}$ fish (Figure 6B; supplemental Figure 7D). On the other hand, injection of *runx1*$^{del8/del8}$;*Tg(cd41:GFP)* embryos with a published *gata2b* splicing morpholino, *gata2b*-MO,[33] led to loss of *cd41*-GFP^{+} cells in AGM and CHT (n = 26/29; supplemental Figure 7E) and a significant decrease of survival at 1 month after injection (supplemental Figure 7F).

The normal survival and the absence of obvious hematopoietic phenotypes in both *gata2b* mutants raised the possibility of compensation by the paralogous gene, *gata2a,* which is also expressed in the aortic endothelium.[34] Using a published CRISPR pair,[34] we deleted the i4 enhancer of *gata2a* (*gata2a*^{i4del194}) in *runx1;gata2b* fish to reduce *gata2a* expression specifically in the hemogenic endothelium (Figure 6C; supplemental Figure 7G). We assessed the hematopoietic phenotype in the triple mutant line (*runx1*^{del8}, *gata2b*^{ins5}, and *gata2a*^{i4del194}). At 15 dpf, the bloodless phenotype was observed only in *runx1*$^{del8/del8}$ larvae, irrespective of *gata2b* and *gata2a* mutation status (supplemental Figure 7H). However, at 1 to 2 months of age, the only fish that remained bloodless (and smaller than their clutchmates) were *runx1* $^{del8/del8}$ with at least 3 *gata2* mutant alleles (*gata2b*$^{+/-}$/*gata2a*$^{-/-}$, *gata2b*$^{-/-}$/*gata2a*$^{+/-}$, or *gata2b*$^{-/-}$/*gata2a*$^{-/-}$; Figure 6D). Moreover, histologic analysis showed that all *runx1*$^{-/-}$ fish with at least 3 *gata2* mutant alleles had no hematopoietic progenitors in their kidneys (Figure 6E). These findings clearly indicated that *gata2a* and *gata2b* were required for the hematopoietic recovery in the *runx1* nulls. Interestingly, hematopoiesis appeared normal in the kidneys of *runx1*^{wt};*gata2b*$^{-/-}$;*gata2a*$^{-/-}$ fish. Although we could not exclude the presence of lineage-specific defects in the absence of GATA2,

Figure 5. *Gata2* is upregulated in the HSPCs of *Runx1* zebrafish and mice knockouts. (A) Stream plot representing the pseudotime trajectory projection of wild-type *cd41*:GFP^{low} cells at 6, 10, and 16 dpf and their different identities. (B) Subway map depicting the distribution of wild-type *cd41*:GFP^{low} cells from different time points to the different branches. (C) Stream plot representing the pseudotime trajectory projection of *runx1*$^{del8/del8}$ *cd41*:GFP^{low} cells at 6, 10, and 16 dpf and their different identities. (D) Subway map illustrating the contribution of *runx1*$^{del8/del8}$ *cd41*:GFP^{low} at different time points to the different branches. (E) Venn diagram representing the number of upregulated genes in *runx1*$^{del8/del8}$ HSC/HSPCs vs wild-type at 6, 10, and 16 dpf ($P_{adj} < .05$, FC > 1.5). Sixty-one genes were commonly upregulated, of which 8 were transcription factors (listed). (F) Stream plot depicting the expression of *gata2b* in the *runx1*$^{del8/del8}$ larval cd41-GFP^{low} pseudotime development (from panels C and D). See supplemental Figure 5 for additional analyses of hematopoietic differentiation trajectories in *runx1*$^{del8/del8}$ and wild-type larvae at 6, 10, and 16 dpf. (G) Unsupervised hierarchical clustering of wild-type and *Runx1*$^{-un}$ RNAseq samples and heat map depicting the differentially expressed genes between wild-type and *Runx1*$^{-un}$ c-Kit^{+} HSPCs (940 downregulated and 414 upregulated in the *Runx1*$^{-un}$; $P_{adj} < .05$, FC > 2). (H) Top transcription factors enriched for regulating the differentially expressed genes. The x axis of the heatmap lists the transcription factors, and the y axis shows the DE genes sorted in the same order of the y axis in panel B. Bar plot on the top showed the enrichment *P* values for each transcription factor. (I) *Gata2* expression in c-kit^{+} bone marrow cells in control and *Runx1*$^{-/-}$ mice, measured by RNA-seq. Round and triangle points mark transcripts per kilobase million values of each mouse in control and *Runx1*$^{-/-}$ mice, respectively. Red ticks mark the average transcripts per kilobase million value. See supplemental Figure 6 for additional data on *Gata2* expression in *Runx1* conditional knockout mice.

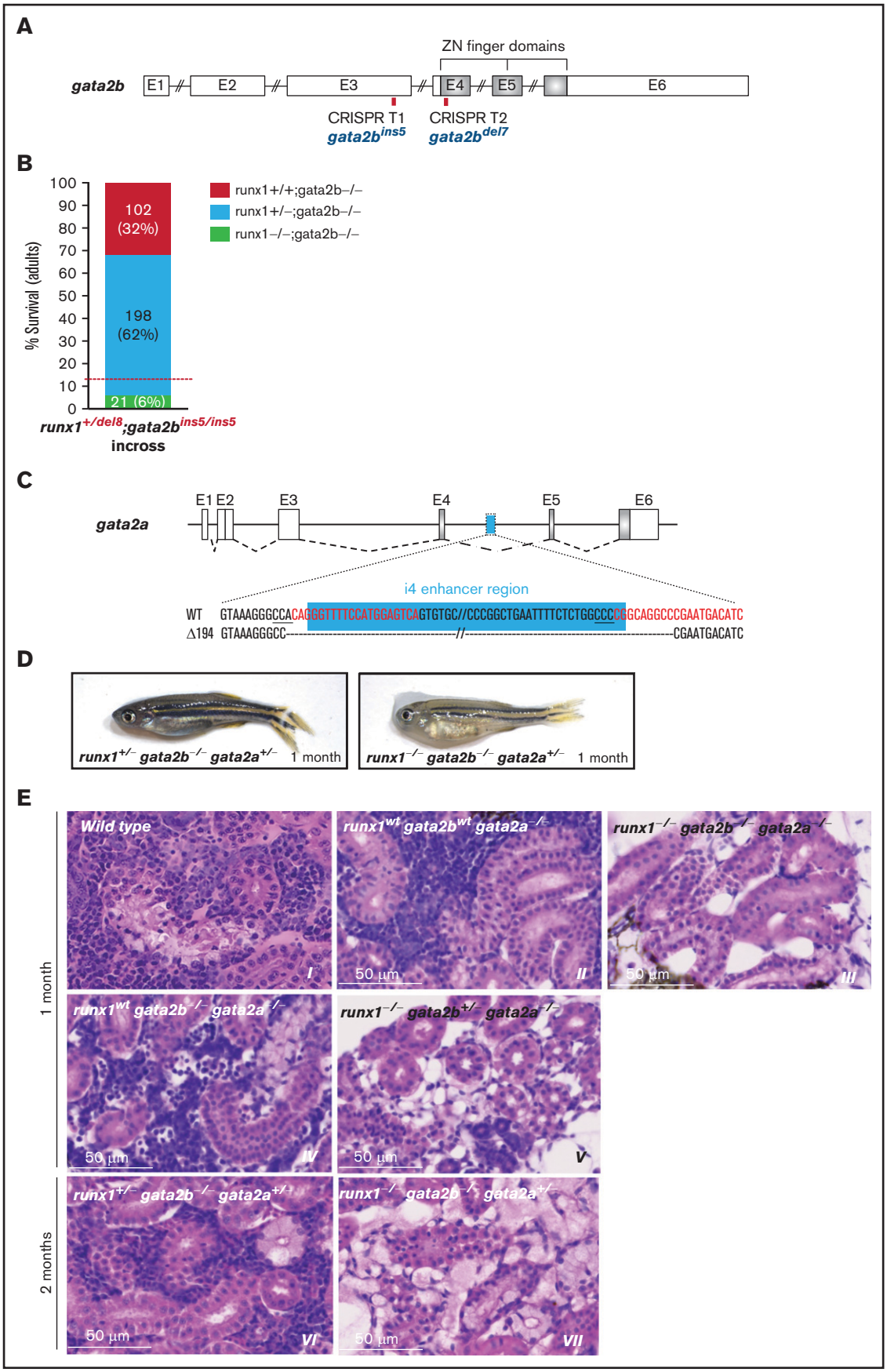
A
ZN finger domains
gata2b
E1
E2
E3
E4
E5
E6
CRISPR T1
gata2b^ins5
CRISPR T2
gata2b^del7
B
% Survival (adults)
runx1+/+;gata2b–/–
runx1+/–;gata2b–/–
runx1–/–;gata2b–/–
102 (32%)
198 (62%)
21 (6%)
runx1^+/del8;gata2b^ins5/ins5 incross
C
gata2a
E1 E2
E3
E4
E5
E6
i4 enhancer region
WT GTAAAGGGCCACAGGGTTTTCCATGGAGTCAGTGTGC//CCCGGCTGAATTTTCTCTGGCCCCGGCAGGCCCGAATGACATC
Δ194 GTAAAGGGCC----------//----------CGAATGACATC
D
runx1+/– gata2b–/– gata2a+/– 1 month
runx1–/– gata2b–/– gata2a+/– 1 month
E
1 month
2 months
Wild type
I
runx1wt gata2bwt gata2a–/–
II
runx1–/– gata2b–/– gata2a–/–
III
runx1wt gata2b–/– gata2a–/–
IV
runx1–/– gata2b+/– gata2a–/–
V
runx1+/– gata2b–/– gata2a+/–
VI
runx1–/– gata2b–/– gata2a+/–
VII
50 µm

Figure 6.

our data suggest that definitive hematopoiesis could proceed without *gata2* (Figure 6E).

Discussion

The 3 new zebrafish *runx1*$^{-/-}$ lines and the previously reported *runx1*$^{W84X/W84X}$ failed to initiate definitive hematopoiesis during early embryonic development, but between 30% and 40% of the *runx1*$^{-/-}$ larvae could regain hematopoiesis and survive to fertile adults. These findings definitely proved the presence of a RUNX1-independent mechanism for HSC production and definitive hematopoiesis. Interestingly, the expression profile of *runx1*$^{-/-}$ adult kidney cells was relatively normal except for the thrombocyte lineage, which is dependent on RUNX1.[14,35,36]

We observed *cd41*:GFP^{low} cells in the AGM of *runx1*$^{-/-}$ embryos at 2.5 dpf, which were derived from hemogenic endothelium and possessed HSC-like gene expression profile. *cd41*:GFP^{low} HSC/HSPCs were later expanded in the kidney of *runx1*$^{-/-}$ larvae during the visible recovery of circulating blood cells. Therefore, we hypothesize that these *cd41*:GFP^{low} HSC/HSPCs are responsible for hematopoiesis recovery in *runx1*$^{-/-}$ larvae.

We characterized the *cd41*:GFP^{low} HSC/HSPCs in the *runx1*$^{-/-}$ larvae by scRNA-seq. At all stages, these cells differed significantly from wild-type cells in levels of heterogeneity and expression profile, with identification of signature genes unique to *runx1*$^{-/-}$ *cd41*:GFP^{low} HSC/HSPCs. In fact, the cd41:GFP^{low} HSC/HSPCs in the *runx1*$^{-/-}$ larvae clustered separately from the wild-type HSC/HSPCs at all stages, suggesting that they have a unique aberrant phenotype rather than having a developmental delay or block. Trajectory analysis across 3 larval stages demonstrated that *runx1*$^{-/-}$ *cd41*:GFP^{low} cells were skewed toward earlier stages of development. At 10 and 16 dpf, contributions to the development of the erythroid and myeloid branches could be observed in the *runx1*$^{del8/del8}$, probably representing the hematopoietic expansion during the recovery period. *runx1*$^{del8/del8}$ larvae appeared to have a large number of *cd41*:GFP^{low} erythroid progenitors, although cd41:GFP is not known to be expressed in erythroid cells.[17,29,37] We speculate that these erythroid progenitors were recently generated from the GFP^{low} HSC/HSPCs and therefore still retained GFP expression.

To uncover the mechanism for RUNX1-independent hematopoiesis, we focused our attention on transcription factors differentially upregulated in the *runx1*$^{-/-}$ HSC/HSPCs. *gata2b* was the only transcription factor upregulated at all larval stages and in the kidney of *runx1*$^{-/-}$ adults. Importantly, *gata2a* was not differentially expressed in the *runx1*$^{-/-}$ at any time point. GATA2 is required for HSC development and is known to act upstream of RUNX1 in the hemogenic endothelium.[8,38,39] Zebrafish contain 2 *GATA2* paralogs, *gata2a*, which is expressed in the whole vasculature including hemogenic endothelium,[34] and *gata2b*, which is specifically expressed in hemogenic endothelium.[33] A previous publication showed that, at the onset of definitive hematopoiesis, *gata2a*$^{\Delta i4/\Delta i4}$ mutants present an initial delay in the induction of hemogenic endothelium but then can progress with a normal hematopoietic development.[34]

gata2b mutants, on the other hand, present a reduction in HSC at the onset of definitive hematopoiesis and have defects in neutrophil and monocytic differentiation lineages as adults.[40]

Surprisingly, there were no obvious hematopoietic defects in the adult *gata2b*$^{-/-}$;*gata2a*$^{-/-}$ fish, suggesting GATA2 is not required for hematopoiesis.[34] However, recovery of definitive hematopoiesis in *runx1*$^{-/-}$ fish was completely abolished in the absence of at least 3 of the 4 *gata2a/2b* alleles. Our results show that GATA2 is responsible for RUNX1-independent hematopoiesis. Moreover, the results suggest that GATA2 and RUNX1 complement each other for their respective roles during hematopoiesis. Although there have been reports that they work synergistically,[41] our findings suggest that they can work independently, providing redundant mechanisms for HSC production.

It has been reported that CD41^{+} pre-HSCs can be found in the ventral dorsal aorta of the *Runx1*^{ko} mice around E10.5.[42] Based on our analyses, *Gata2* did not appear to be upregulated in the AGM of the *Runx1*^{ko} mice. However, *Gata2* is upregulated and identified as the top upstream regulator of the differentially expressed genes in the c-Kit^{+} HSPCs in adult *Runx1*$^{-/-}$ mice. Therefore, it is possible that a RUNX1-independent hematopoiesis initiates in both zebrafish and mice, but this process is successful only in zebrafish because of its larvae can survive in the absence of blood circulation. Because of this mechanism, several other bloodless mutants in the zebrafish could be partially or completely rescued through compensating mechanisms.[43-46]

Moreover, RUNX1 and GATA2 may interact with each other for leukemia development. As transcription factors, RUNX1 and GATA2 can interact with each other directly and form DNA-binding complexes.[41] RUNX1 and GATA2 binding sites are found on a number of hematopoietic genes, and these 2 transcription factors have been shown to cooperate with other transcription factors to regulate genes considered critical for the balance between quiescence and proliferation of HSCs,[41] as well as genes involved in leukemia.[47] We recently found that *GATA2* is frequently deleted in human CBF leukemias, those that are associated with *RUNX1* and *CBFB* fusion genes.[48] In addition, we demonstrated that *Gata2* contributes to leukemogenesis associated with *CBFB-MYH11* in a mouse model.[49] Interestingly, we also demonstrated that *Runx1* is required for leukemogenesis associated with *CBFB-MYH11* in mouse models,[50] raising the possibility that *Gata2* and *Runx1* function synergistically during leukemogenesis.

Figure 6. *gata2b* and *gata2a* are required for the development of definitive hematopoiesis in *runx1* mutants. (A) Schematic representation of the *gata2b* gene showing the CRISPR targets T1 and T2 (red bars) used to generate the *gata2b*^{ins5} and the *gata2b*^{del7} mutant lines. (B) Survival of adult *runx1*^{del8}/*gata2b*^{ins5} double mutants obtained from the incross of *runx1*$^{+/del8}$; *gata2b*$^{ins5/ins5}$ fish. Red dashed lines indicate the expected ratio of *runx1*$^{-un}$ recovery based on our previous experimental data (Figure 1E). Each bar segment shows the percentage and number of fish recovered for each genotype. (C) Schematic representation of *gata2a* genomic structure. The cyan box represents the 150-bp i4 enhancer that was removed using 2 CRISPR guides (red letters). (D) Photographs of representative 1-month-old *runx1*$^{+/-}$*gata2b*$^{-at}$*gata2a*$^{+/-}$ and *runx1*$^{-un}$*gata2b*$^{-at}$*gata2a*$^{-at}$ fish, with the latter more pale and smaller than the former. (E) Histologic analysis of kidney marrow of triple mutants *runx1*^{del8};*gata2b*^{ins5};*gata2a*^{i4del1} at 1 or 2 months. Kidneys from runx1 wild-type and *runx1*$^{+/-}$ fish (panels II, IV, and VI) are similar to the kidney from the wild-type control (panel I) with marrows populated by blood progenitors. Kidneys from *runx1*$^{del8/del8}$ fish with *gata2b*$^{-at}$*gata2a*$^{-at}$ (III), *gata2b*$^{+/-}$*gata2a*$^{-at}$ (V), or *gata2b*$^{+/-}$*gata2a*$^{+/-}$ (VII) completely lack blood progenitors. See supplemental Figure 7 for additional characterizations of the zebrafish *gata2b* and *gata2a* mutants.

Overall, our data suggest that GATA2 serves as a safeguard for the formation of definitive HSCs/HSPCs in case RUNX1 is inactivated and that this mechanism is evolutionary conserved. It may not be surprising that GATA2 serves this role because both GATA2 and RUNX1 are key transcription factors for hematopoiesis. The interaction between RUNX1 and GATA2 at common target genes has previously been reported, and interestingly, *Gata2*$^{+/-}$*Runx1*$^{+/-}$ mice are embryonic lethal with hematopoietic defects.[41] However, it is surprising that GATA2 can bypass RUNX1 to establish functional hematopoiesis. Likewise, RUNX1 seems to be able to sustain hematopoiesis in the absence of GATA2. Only when losing both RUNX1 and at least 75% of GATA2 was hematopoiesis abolished, suggesting remarkable redundancy between GATA2 and RUNX1 to ensure the initiation and maintenance of HSC that can support hematopoiesis, a vital system for the survival of vertebrate animals.

Acknowledgments

The authors thank the National Institutes of Health (NIH) Intramural Sequencing Center (NISC) for A-seq of the kidney samples; Brant Weinstein for the *Tg(kdrl:mCherry)* fish line; all Liu laboratory members, Alberto Rissone, and Aniket Gore for helpful discussion and advice; and Faiza Naz for support with single cell cDNA synthesis.

The work described in this paper was supported by the Intramural Research Programs at the National Human Genome Research Institute, NIH, and the National Institute of Arthritis and Musculoskeletal and Skin Diseases, NIH. This work used the computational resources of the NIH HPC Biowulf cluster (http://hpc.nih.gov).

Authorship

Contribution: E. Bresciani, B.C., K.B., V.S.G., and E. Broadbridge designed and performed the experiments and analyzed the data; E. Bresciani, R.S., and P.L. designed and organized the experiments and analyzed the data; M.K. assisted with fluocytometry; U.H. assisted with genotyping; S.W. assisted with microscopy; S.D. and V.S. assisted with capture and sequencing of 10× genomics and provided technical support; T.Z. designed and performed mouse experiments; E. Bresciani, E.M.K., and K.Y. performed bioinformatic analysis; E. Bresciani and P.L. wrote the manuscript.

Conflict-of-interest disclosure: The authors declare no competing financial interests.

ORCID profiles: K.Y., 0000-0002-2561-8160; M.K., 0000-0001-7157-7964; R.S., 0000-0001-5565-662X; P.L., 0000-0002-6779-025X.

Correspondence: Paul Liu, 50 South Dr, Bldg 50, Rm 5222C, NHGRI, NIH, Bethesda, MD 20892; e-mail: pliu@mail.nih.gov.

References

1. Bresciani E, Carrington B, Wincovitch S, et al. CBFβ and RUNX1 are required at 2 different steps during the development of hematopoietic stem cells in zebrafish. *Blood.* 2014;124(1):70-78.
2. Okuda T, van Deursen J, Hiebert SW, Grosveld G, Downing JR. AML1, the target of multiple chromosomal translocations in human leukemia, is essential for normal fetal liver hematopoiesis. *Cell.* 1996;84(2):321-330.
3. Sasaki K, Yagi H, Bronson RT, et al. Absence of fetal liver hematopoiesis in mice deficient in transcriptional coactivator core binding factor beta. *Proc Natl Acad Sci USA.* 1996;93(22):12359-12363.
4. Wang Q, Stacy T, Binder M, Marin-Padilla M, Sharpe AH, Speck NA. Disruption of the Cbfa2 gene causes necrosis and hemorrhaging in the central nervous system and blocks definitive hematopoiesis. *Proc Natl Acad Sci USA.* 1996;93(8):3444-3449.
5. Wang Q, Stacy T, Miller JD, et al. The CBFbeta subunit is essential for CBFalpha2 (AML1) function in vivo. *Cell.* 1996;87(4):697-708.
6. Tsai FY, Keller G, Kuo FC, et al. An early haematopoietic defect in mice lacking the transcription factor GATA-2. *Nature.* 1994;371(6494):221-226.
7. Ling KW, Ottersbach K, van Hamburg JP, et al. GATA-2 plays two functionally distinct roles during the ontogeny of hematopoietic stem cells. *J Exp Med.* 2004;200(7):871-882.
8. de Pater E, Kaimakis P, Vink CS, et al. Gata2 is required for HSC generation and survival. *J Exp Med.* 2013;210(13):2843-2850.
9. Kaimakis P, de Pater E, Eich C, et al. Functional and molecular characterization of mouse Gata2-independent hematopoietic progenitors. *Blood.* 2016; 127(11):1426-1437.
10. Leubolt G, Redondo Monte E, Greif PA. GATA2 mutations in myeloid malignancies: Two zinc fingers in many pies. *IUBMB Life.* 2020;72(1):151-158.
11. Chen MJ, Yokomizo T, Zeigler BM, Dzierzak E, Speck NA. Runx1 is required for the endothelial to haematopoietic cell transition but not thereafter. *Nature.* 2009;457(7231):887-891.
12. Liakhovitskaia A, Rybtsov S, Smith T, et al. Runx1 is required for progression of CD41+ embryonic precursors into HSCs but not prior to this. *Development.* 2014;141(17):3319-3323.
13. Jin H, Sood R, Xu J, et al. Definitive hematopoietic stem/progenitor cells manifest distinct differentiation output in the zebrafish VDA and PBI. *Development.* 2009;136(4):647-654.
14. Sood R, English MA, Belele CL, et al. Development of multilineage adult hematopoiesis in the zebrafish with a runx1 truncation mutation. *Blood.* 2010; 115(14):2806-2809.
15. Monte W . *The Zebrafish Book: A Guide for the Laboratory Use of Zebrafish (Danio rerio).* Eugene, OR: University of Oregon; 1995.

16. Traver D, Paw BH, Poss KD, Penberthy WT, Lin S, Zon LI. Transplantation and in vivo imaging of multilineage engraftment in zebrafish bloodless mutants. *Nat Immunol.* 2003;4(12):1238-1246.

17. Lin HF, Traver D, Zhu H, et al. Analysis of thrombocyte development in CD41-GFP transgenic zebrafish. *Blood.* 2005;106(12):3803-3810.

18. Jung HM, Castranova D, Swift MR, et al. Development of the larval lymphatic system in zebrafish. *Development.* 2017;144(11):2070-2081.

19. Kim D, Paggi JM, Park C, Bennett C, Salzberg SL. Graph-based genome alignment and genotyping with HISAT2 and HISAT-genotype. *Nat Biotechnol.* 2019;37(8):907-915.

20. Anders S, Pyl PT, Huber W. HTSeq: a Python framework to work with high-throughput sequencing data. *Bioinformatics.* 2015;31(2):166-169.

21. Tripathi S, Pohl MO, Zhou Y, et al. Meta- and orthogonal integration of influenza "OMICs" data defines a role for UBR4 in virus budding. *Cell Host Microbe.* 2015;18(6):723-735.

22. Stuart T, Butler A, Hoffman P, et al. Comprehensive integration of single-cell data. *Cell.* 2019;177(7):1888-1902.

23. Stuart T, Satija R. Integrative single-cell analysis. *Nat Rev Genet.* 2019;20(5):257-272.

24. Chen H, Albergante L, Hsu JY, et al. Single-cell trajectories reconstruction, exploration and mapping of omics data with STREAM. *Nat Commun.* 2019; 10(1):1903.

25. Growney JD, Shigematsu H, Li Z, et al. Loss of Runx1 perturbs adult hematopoiesis and is associated with a myeloproliferative phenotype. *Blood.* 2005; 106(2):494-504.

26. Kühn R, Schwenk F, Aguet M, Rajewsky K. Inducible gene targeting in mice. *Science.* 1995;269(5229):1427-1429.

27. Lewandoski M, Martin GR. Cre-mediated chromosome loss in mice. *Nat Genet.* 1997;17(2):223-225.

28. Zhen T, Kwon EM, Zhao L, et al. *Chd*7 deficiency delays leukemogenesis in mice induced by *Cbfb-MYH11. Blood.* 2017;130(22):2431-2442.

29. Macaulay IC, Svensson V, Labalette C, et al. Single-cell RNA-sequencing reveals a continuous spectrum of differentiation in hematopoietic cells. *Cell Rep.* 2016;14(4):966-977.

30. Bertrand JY, Kim AD, Violette EP, Stachura DL, Cisson JL, Traver D. Definitive hematopoiesis initiates through a committed erythromyeloid progenitor in the zebrafish embryo. *Development.* 2007;134(23):4147-4156.

31. Ganis JJ, Hsia N, Trompouki E, et al. Zebrafish globin switching occurs in two developmental stages and is controlled by the LCR. *Dev Biol.* 2012;366(2): 185-194.

32. Fei DL, Zhen T, Durham B, et al. Impaired hematopoiesis and leukemia development in mice with a conditional knock-in allele of a mutant splicing factor gene *U2af1. Proc Natl Acad Sci USA.* 2018;115(44):E10437-E10446.

33. Butko E, Distel M, Pouget C, et al. Gata2b is a restricted early regulator of hemogenic endothelium in the zebrafish embryo. *Development.* 2015;142(6): 1050-1061.

34. Dobrzycki T, Mahony CB, Krecsmarik M, et al. Deletion of a conserved Gata2 enhancer impairs haemogenic endothelium programming and adult Zebrafish haematopoiesis. *Commun Biol.* 2020;3(1):71.

35. Song WJ, Sullivan MG, Legare RD, et al. Haploinsufficiency of CBFA2 causes familial thrombocytopenia with propensity to develop acute myelogenous leukaemia. *Nat Genet.* 1999;23(2):166-175.

36. Ichikawa M, Asai T, Saito T, et al. AML-1 is required for megakaryocytic maturation and lymphocytic differentiation, but not for maintenance of hematopoietic stem cells in adult hematopoiesis [correction published in *Nat Med.* 2005;11;102]. *Nat Med.* 2004;10(3):299-304.

37. Ma D, Zhang J, Lin HF, Italiano J, Handin RI. The identification and characterization of zebrafish hematopoietic stem cells. *Blood.* 2011;118(2):289-297.

38. Gao X, Johnson KD, Chang YI, et al. Gata2 cis-element is required for hematopoietic stem cell generation in the mammalian embryo. *J Exp Med.* 2013; 210(13):2833-2842.

39. Lim KC, Hosoya T, Brandt W, et al. Conditional Gata2 inactivation results in HSC loss and lymphatic mispatterning. *J Clin Invest.* 2012;122(10):3705-3717.

40. Gioacchino E, Koyunlar C, Zink J, et al. Essential role for Gata2 in modulating lineage output from hematopoietic stem cells in zebrafish. *Blood Adv.* 2021;5(13):2687–2700.

41. Wilson NK, Foster SD, Wang X, et al. Combinatorial transcriptional control in blood stem/progenitor cells: genome-wide analysis of ten major transcriptional regulators. *Cell Stem Cell.* 2010;7(4):532-544.

42. Vink CS, Calero-Nieto FJ, Wang X, et al. Iterative single-cell analyses define the transcriptome of the first functional hematopoietic stem cells. *Cell Rep.* 2020;31(6):107627.

43. Lyons SE, Lawson ND, Lei L, Bennett PE, Weinstein BM, Liu PP. A nonsense mutation in zebrafish gata1 causes the bloodless phenotype in vlad tepes. *Proc Natl Acad Sci USA.* 2002;99(8):5454-5459.

44. Belele CL, English MA, Chahal J, et al. Differential requirement for Gata1 DNA binding and transactivation between primitive and definitive stages of hematopoiesis in zebrafish. *Blood.* 2009;114(25):5162-5172.

45. Liao EC, Trede NS, Ransom D, Zapata A, Kieran M, Zon LI. Non-cell autonomous requirement for the bloodless gene in primitive hematopoiesis of zebrafish. *Development.* 2002;129(3):649-659.

46. Soza-Ried C, Hess I, Netuschil N, Schorpp M, Boehm T. Essential role of c-myb in definitive hematopoiesis is evolutionarily conserved. *Proc Natl Acad Sci USA.* 2010;107(40):17304-17308.

47. Pippa R, Dominguez A, Malumbres R, et al. MYC-dependent recruitment of RUNX1 and GATA2 on the SET oncogene promoter enhances PP2A inactivation in acute myeloid leukemia. *Oncotarget.* 2016;8(33):53989-54003.

48. Sood R, Hansen NF, Donovan FX, et al. Somatic mutational landscape of AML with inv(16) or t(8;21) identifies patterns of clonal evolution in relapse leukemia. *Leukemia.* 2016;30(2):501-504.

49. Saida S, Zhen T, Kim E, et al. Gata2 deficiency delays leukemogenesis while contributing to aggressive leukemia phenotype in Cbfb-MYH11 knockin mice. *Leukemia.* 2020;34(3):759-770.

50. Zhen T, Cao Y, Ren G, et al. RUNX1 and CBFβ-SMMHC transactivate target genes together in abnormal myeloid progenitors for leukemia development. *Blood.* 2020;136(21):2373-2385.